ORGANIC PROCESS RESEARCH & DEVELOPMENT
OPR&D

pubs.acs.org/OPRD

Article

A Virtual Plant for Integrated Continuous Manufacturing of a Carfilzomib Drug Substance Intermediate, Part 1: CDI-Promoted Amide Bond Formation

Elçin Içten,* Andrew J. Maloney, Matthew G. Beaver, Dongying Erin Shen, Xiaoxiang Zhu, Lauren R. Graham, Jo Anna Robinson, Seth Huggins, Ayman Allian, Roger Hart, Shawn D. Walker, Pablo Rolandi, and Richard D. Braatz

Cite This: *Org. Process Res. Dev.* 2020, 24, 1861−1875

Read Online

ACCESS | Metrics & More | Article Recommendations

ABSTRACT: This article details process characterization efforts and the development of corresponding process models to inform a process control strategy to produce a carfilzomib drug substance intermediate, morpholine amide **3**. Model calibration for relevant unit operations and development of a dynamic integrated flowsheet-level model in gPROMS FormulatedProducts software allowed an investigation of the impact of process disturbances and model uncertainties on critical quality attributes (CQAs) and identification of critical process disturbances and failure modes to guide the process control strategy. The main CQA for this step was the conversion of Boc-D-leucine monohydrate (≥95%). The model was used to ensure that a state of control would be maintained in the presence of disturbances to target process parameters. The process was found to be robust against the analyzed disturbance scenarios, including worst-case combined disturbances. One case study highlights the dynamics of flow blockage for a key reagent, *N*,*N*′-carbonyldiimidazole (CDI), resulting from line clogging and the relationship between blockage duration and reaction conversion. The blockage was studied in silico, and the model demonstrated that the acceptance criteria for reaction conversion were met even with a flow rate reduction of 40%. The detrimental impact on the product concentration in the downstream process, however, required modification of the final distillation operation. The revised distillation column operation was demonstrated to address this concern and tolerated variable concentrations of morpholine amide while achieving the target water specification (<0.25 wt %). The results of this in silico analysis were verified with a production-scale demonstration of morpholine amide synthesis at a throughput of 12 kg/day to experimentally evaluate the impact of disturbances on the control strategy and overall performance of the system.

KEYWORDS: *continuous pharmaceutical manufacturing, process systems engineering, process control, process modeling, rapid process development, flow chemistry*

1. INTRODUCTION

The drive for continuous manufacturing (CM) of pharmaceuticals has grown rapidly, with industry, academia, and regulatory agencies highlighting the requirements of such a change.[1−3] Continuous manufacturing is a compelling mode of operation with many benefits, including (1) reduced equipment sizing, footprint, and therefore capital investment in facilities, (2) increased process flexibility through the use of modular equipment and platformed unit operations to support integrated processes and multiple products, (3) agility to meet "just in time" demand and reduce inventory, (4) improved environmental sustainability through reduced material consumption and waste generation during process development, (5) improved process safety due to better heat and mass transfer, thus enabling the investigation of novel chemical transformations, (6) the potential for more rapid technology transfers due to similarities in scale and equipment from development to manufacture, and (7) improved process control via integration of on-line measurement and sensing via process analytical technology (PAT) tools and application of quality by design (QbD) and recently introduced quality by control (QbC) frameworks to achieve real-time quality control.[4−11]

Many examples of the implementation of continuous single unit operations (e.g., reactions or crystallization) exist; however, examples of connected unit operations are less prevalent. In an academic setting, Mascia et al. presented the first example of an integrated continuous synthesis, purification, and final dosage formulation of aliskiren hemifumarate.[12] Zhang et al. demonstrated the continuous synthesis and purification of ciprofloxacin hydrochloride, neostigmine methylsulfate, and rufinamide.[13] In an industrial context, many companies have demonstrated improved capabilities and

Special Issue: Flow Chemistry Enabling Efficient Synthesis

Received: April 15, 2020
Published: July 14, 2020

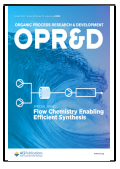

https://dx.doi.org/10.1021/acs.oprd.0c00187
Org. Process Res. Dev. 2020, 24, 1861−1875

investment to develop continuous processes for isolated unit operations, including reactions[14−17] and separation and crystallization[18] unit operations. The development of end-to-end processes has also demonstrated, including Eli Lilly and Company's kilogram-scale delivery of prexasertib monolactate monohydrate and merestinib for use in human clinical trials under cGMP conditions in their small-volume continuous manufacturing facility[19−21] and a collaboration between industry and the U.S. Food and Drug Administration (FDA) for integrated continuous manufacturing from synthesis of active pharmaceutical ingredients through final oral dosage forms.[22]

Despite the advantages attributed to continuous processing of synthetic drug substances, wider adoption across industry is still limited by the complexity of this mode of operation relative to traditional batch processing. The transition from batch mode to a continuous mode of operation, especially for connected processes, significantly expands the number of process parameters that require evaluation for optimal process design and process characterization. Our approach augments empirical design with process modeling, identifying key process relationships with carefully designed experiments and developing mechanistic understanding to build the design space for integrated processes. Process modeling to improve process understanding and ensure product quality is an approach that has been adopted in continuous drug substance manufacturing and drug product manufacturing.[23−25] This drive to apply process modeling to continuous manufacturing enables deeper process understanding and the development of robust control strategies.[26−28]

Described herein is the development of a virtual plant for synthetic continuous drug substance manufacturing to enable a process control strategy for end-to-end continuous manufacturing and facilitate technology transfer to manufacturing facilities while reducing resource requirements by relying more on in silico experiments. A virtual plant was developed to support the continuous manufacture of (*S*,*R*)-epoxy ketone **1**, a drug substance intermediate in the synthesis of carfilzomib (Kyprolis) (Scheme 1). Data-rich experiments were executed

Scheme 1. Chemical Structures of Carfilzomib and (*S*,*R*)-Epoxy Ketone 1

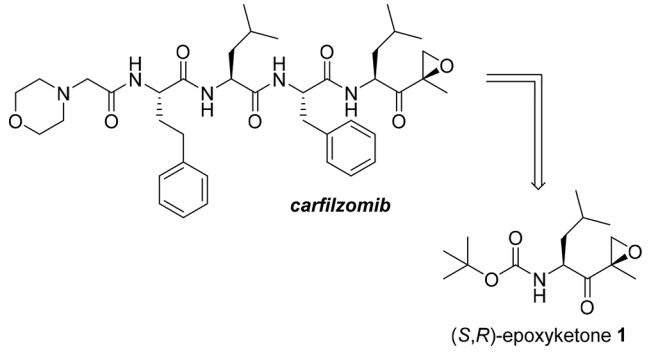

to gain mechanistic understanding of each unit operation independently. Individual unit operation models were integrated in the gPROMS platform to develop end-to-end process understanding through detailed modeling of relevant physical and chemical phenomena. The integrated-systems-based model used in the in silico experiments allowed for identification of critical process parameters that affect critical quality attributes and greater understanding of the design space that maintains a state of control. These dynamic models were then used to inform an integrated process control strategy that was envisioned to support technology transfer, process qualification, and regulatory filings for continuous manufacturing processes.

This three-part publication series introduces the experimental characterization, process model development, end-to-end simulation, and disturbance analysis for the manufacture of (*S*,*R*)-epoxy ketone **1** by the four-step sequence depicted in Scheme 2, a continuous operation comprising 27 unit operations. Part 1 of this series focuses on the development of a continuous flow process to produce morpholine amide **3** from Boc-D-leucine monohydrate (**2**). Part 2 of the series (10.1021/acs.oprd.0c00188)[29] describes the development of a continuous Barbier-type Grignard process to produce enone **4** from morpholine amide **3**. Part 3 of the series (10.1021/acs.oprd.0c00189)[30] describes the manganese-catalyzed asymmetric epoxidation of enone **4** and further purification of (*R*,*R*)-epoxy ketone **5** via crystallization. Process development was supported using first-principles-based mathematical process models and process simulation to understand the impact of competing effects on the underlying chemistry and to develop a robust process control strategy for the end-to-end process.

2. PROCESS OVERVIEW FOR CONTINUOUS MANUFACTURE OF A KYPROLIS DRUG SUBSTANCE INTERMEDIATE (*S*,*R*)-EPOXYKETONE

Amgen's Drug Substance Technologies Process Development team developed a continuous process for the manufacture of a Kyprolis drug substance intermediate, *tert*-butyl ((*S*)-4-methyl-1-((*R*)-2-methyloxiran-2-yl)-1-oxopentan-2-yl)carbamate or (*S*,*R*)-epoxy ketone **1**. Kyprolis is a proteasome inhibitor indicated for the treatment of patients with relapsed or refractory multiple myeloma. Kyprolis was initially approved through the FDA's accelerated approval pathway in 2012 on the basis of a pivotal phase II trial which was progressed by Proteolix and Onyx Pharmaceuticals.[31] Amgen acquired Kyprolis in 2013, and Drug Substance Technologies initiated process development strategies to improve the original development route of epoxy ketone intermediate **1** to ensure commercial supply.[32] Subsequently, an improved route was developed to improve the yield and environmental sustainability and reduce the cost of goods significantly.[33] The improved route prompted our team to explore the use of continuous processing because of the highly exothermic Grignard chemistry, epoxidation reaction, and fast reaction kinetics as well as the low volume requirements.

The four-step improved process to prepare (*S*,*R*)-epoxy ketone **1** is shown in Scheme 2. The starting material **2** is subjected to *N*,*N*′-carbonyldiimidazole (CDI)-promoted amide bond formation with morpholine in 2-methyltetrahydrofuran (MeTHF) to prepare morpholine amide intermediate **3**. Following aqueous workup, the organic stream is azeotropically distilled to remove residual water, diluted with tetrahydrofuran, and subjected to a Barbier-type Grignard reaction with isopropenylmagnesium bromide generated in situ from 2-bromopropene and magnesium turnings to prepare enone **4**. The crude reaction stream undergoes aqueous workup, is solvent swapped to acetonitrile (ACN), and is telescoped to the Step 3 conditions for manganese-catalyzed asymmetric epoxidation in the presence of a catalytic Mn complex, acetic acid (AcOH), and hydrogen peroxide to

https://dx.doi.org/10.1021/acs.oprd.0c00187
Org. Process Res. Dev. 2020, 24, 1861−1875

Scheme 2. Continuous Process Route for the Synthesis of (*S*,*R*)-Epoxy Ketone 1

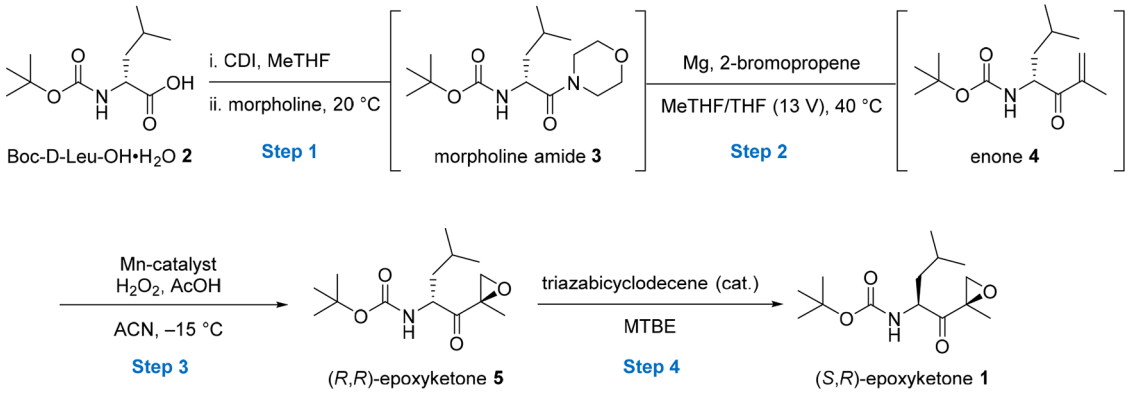

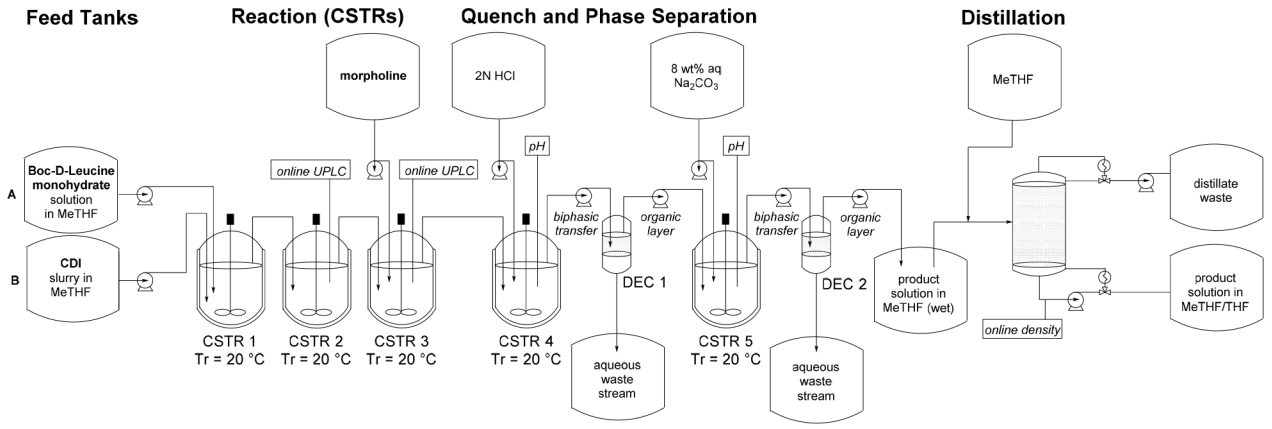

Figure 1. Process flow diagram for the manufacture of morpholine amide.

prepare (*R*,*R*)-epoxy ketone **5**. Residual hydrogen peroxide is quenched with an aqueous solution of sodium bisulfite, and water is added to the organic layer as an antisolvent to crystallize pure **5**. In Step 4, a solution of **5** in methyl *tert*-butyl ether (MTBE) undergoes base-promoted epimerization with triazabicyclodecene (TBD) to generate crude (*S*,*R*)-epoxy ketone **1**. After the residual TBD is quenched with AcOH, the organic stream is solvent-swapped to methanol (MeOH), and water is added as an antisolvent to crystallize pure (*S*,*R*)-epoxy ketone **1**. Full details of the development of this improved process are available in a separate publication.[33]

3. VIRTUAL PLANT DEVELOPMENT FOR MORPHOLINE AMIDE SYNTHESIS

The synthesis of morpholine amide **3** consists of two chemical transformations followed by separation operations; the process flow diagram is illustrated in Figure 1. The process begins with a stream of Boc-D-leucine in MeTHF and a slurry stream of CDI in MeTHF being fed to continuously stirred tank reactor 1 (CSTR1) to form an acylimidazole intermediate. The effluent of CSTR1 is sent to CSTR2 to reach the desired reaction conversion. The intermediate (acylimidazole) produced in CSTR2 is converted to morpholine amide **3** in CSTR3 upon the introduction of morpholine.

In CSTR4, the reaction stream from CSTR3 is subjected to aqueous workup with hydrochloric acid (HCl) to quench the unreacted reagents CDI and morpholine and the byproducts imidazole and acylimidazole, followed by phase separation in decanter 1 (DEC1) to enable removal of quenched species with the aqueous waste stream. In CSTR5, the organic stream from DEC1 is subjected to basic aqueous workup with sodium carbonate to quench unreacted started material Boc-D-leucine, followed by phase separation in DEC2 to enable removal of quenched species with the aqueous waste stream. The effluent of DEC2 is the organic stream containing a product solution in MeTHF, and it is sent to a hold tank until a specified volume is reached. The tank contents are then azeotropically distilled, and the concentrate is diluted with THF and delivered to the downstream unit operations.

All of the unit operations in this process were characterized to build a mechanistic understanding for relevant thermodynamic and physical phenomena. An experimental plan was developed and executed to characterize each unit operation in batch mode while studying the impact of various process conditions and parameters. Parameter estimation was then performed to determine the kinetic and/or thermodynamic model coefficients, and dynamic models were built using integrated process simulation software that is capable of handling dynamic models. Once built, the integrated process models were used for disturbance analysis and control strategy development to meet quality and performance specifications.

3.1. Process Characterization Experiments and Parameter Estimation for Model Development.

3.1.1. Product Formation: Reaction Kinetics and Kinetic Model Development. Reaction kinetic formulation includes three reactions in CSTR1 and CSTR2: (1) the dissociation of crystalline Boc-D-leucine monohydrate to dissolved Boc-D-leucine and water, (2) the reaction of Boc-D-leucine and CDI to form an acylimidazole species and the byproducts imidazole and carbon dioxide, and (3) the reaction of water with CDI to

https://dx.doi.org/10.1021/acs.oprd.0c00187
Org. Process Res. Dev. 2020, 24, 1861−1875

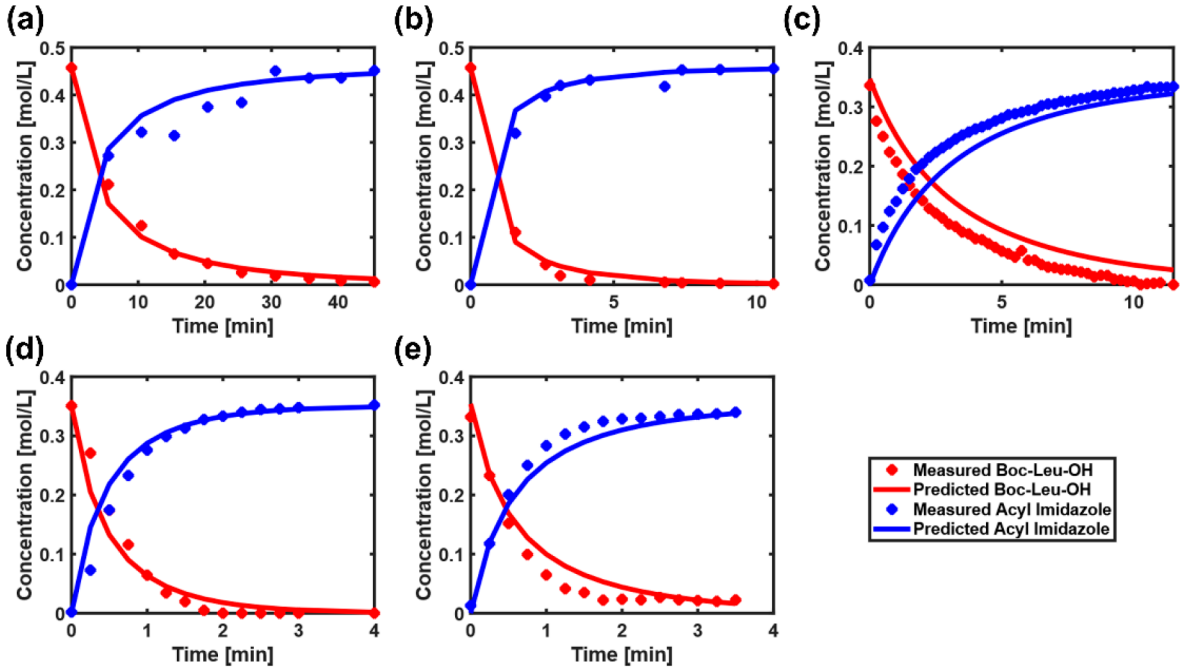

Figure 2. Comparison between model prediction and experimental data for Boc-D-leucine and acylimidazole with initial reaction conditions of (a) 1.2 equiv of CDI, 0 °C, and a feed of dry Boc-D-leucine; (b) 1.2 equiv of CDI, 20 °C, and a feed of dry Boc-D-leucine; (c) 2 equiv of CDI, 0 °C, and a feed of Boc-D-leucine monohydrate; (d) 2 equiv of CDI, 20 °C, and a feed of Boc-D-leucine monohydrate; and (e) 1.5 equiv of CDI, 20 °C, and a feed of Boc-D-leucine monohydrate.

form 2 equiv of imidazole and CO_2. These three reactions are described in eqs 1, 2, and 3, respectively.

$$\text{Boc-D-leucine}\cdot H_2O \rightarrow \text{Boc-D-leucine} + H_2O \quad (1)$$

$$\text{Boc-D-leucine} + \text{CDI} \xrightarrow{k_2} \text{acylimidazole} + \text{imidazole} + CO_2 \quad (2)$$

$$H_2O + \text{CDI} \rightarrow 2\,\text{imidazole} + CO_2 \quad (3)$$

The rate-limiting reaction to prepare the acylimidazole intermediate is described by eq 2, and its progress may be tracked and quantified using analytical tools. A set of batch kinetic experiments were designed and executed to characterize the kinetics of the rate-limiting reaction shown in eq 2; specifically, the temperature (0−20 °C) and equivalents of CDI (1.2−2.0) were varied. Time series data were collected in each experiment to quantify the conversion of Boc-D-leucine and the formation of acylimidazole using ultraperformance liquid chromatography (UPLC) and Fourier transform infrared spectroscopy (FTIR) (Figure 2). In these experiments, the impact of water on the reaction progress was assessed by using an azeotropically distilled Boc-D-leucine feed stream (<500 ppm by Karl Fischer (KF) titration) relative to a feed stream prepared with the monohydrate, as shown in Figure 2a,b and Figure 2c−e, respectively. These experiments confirmed that the kinetics of the rate-limiting reaction was not significantly impacted by the presence of water or dissociation of Boc-D-leucine monohydrate to Boc-D-leucine. The breakdown reaction of Boc-D-leucine monohydrate to Boc-D-leucine and water was confirmed to be instantaneous relative to the rate of acylimidazole formation under the reaction conditions, and an arbitrary high rate constant was assigned for simplicity and to ensure high conversion in the model. The decomposition of CDI (eq 3) was confirmed to occur at a significantly lower rate than the main reaction. Thus, it was assumed to be negligible under the reaction conditions and was not modeled.

The reaction of Boc-D-leucine and CDI to form imidazole, CO_2, and the major product, acylimidazole, was found to follow first-order reaction kinetics with respect to the reactants, and the corresponding reaction rate expression was determined to be that shown in eq 4:

$$r_2 = k_2[\text{Boc-D-leucine}][\text{CDI}] \quad (4)$$

The parameter estimation was performed using DynoChem 5 software by minimizing the sum of squares (SSQ) between the experimental data and model predictions while achieving a 95% confidence interval. The kinetic rate constants for the Arrhenius equation are provided in Table 1.

Table 1. Regressed Kinetic Parameters of the Main Reaction (eq 2) for the Arrhenius Rate Expression (T_{ref} = 20 °C)

parameter	value	95% Confidence Interval (%)	units
k_2	0.0627	6.412	L mol^{-1} s^{-1}
E_2	67.177	5.366	kJ/mol

The reaction kinetic formulation to prepare morpholine amide **3** by the reaction of acylimidazole and morpholine in CSTR3 is described by eq 5:

$$\text{acylimidazole} + \text{morpholine} \rightarrow \text{morpholine amide} + \text{imidazole} \quad (5)$$

This reaction is rapid (<15 s) relative to the reaction shown in eq 2 and reaches complete conversion as confirmed by quantitative UPLC and FTIR. Therefore, the kinetics was not quantified and was assumed to be instantaneous, and an arbitrary high rate constant was assigned for simplicity and to ensure high conversion in the model.

https://dx.doi.org/10.1021/acs.oprd.0c00187
Org. Process Res. Dev. 2020, 24, 1861−1875

3.1.2. Workup Steps: Reaction Kinetics, Liquid–Liquid Extractions and Mass Transfer Kinetics, and Model Development. Reaction kinetic formulation for the aqueous workup includes four reactions that occur within CSTR4: (1) the reaction of imidazole with HCl to form the imidazole·HCl salt, (2) the reaction of morpholine with HCl to form the morpholine·HCl salt, (3) the reaction of unreacted acylimidazole with water to form Boc-D-leucine and imidazole, and (4) the reaction of water with excess CDI to form 2 equiv of imidazole and CO_2. These four reactions are described in eqs 6, 7, 8, and 3, respectively.

$$\text{HCl} + \text{imidazole} \rightarrow \text{imidazole·HCl} \quad (6)$$

$$\text{HCl} + \text{morpholine} \rightarrow \text{morpholine·HCl} \quad (7)$$

$$\text{acylimidazole} + \text{H}_2\text{O} \rightarrow \text{Boc-D-leucine} + \text{imidazole} \quad (8)$$

All of these reactions were confirmed to be fast under acidic reaction conditions (<1 min) and reached complete conversion, as also confirmed in the mass transfer kinetics experiments described below. Therefore, the kinetics was not quantified and assumed to be instantaneous, and an arbitrary high rate constant was assigned for simplicity and to ensure high conversion in the model. This assumption is supported by the relatively small increase in scale in the transition from batch development experiments (100 mL) to production-scale CSTRs (<2 L).

Following the aqueous quench in CSTR4, the biphasic stream undergoes a liquid–liquid phase separation in DEC1. Two sets of batch experiments were designed and executed to characterize the liquid–liquid phase separation and the kinetics of mass transfer between the aqueous and organic layers. These experiments aimed to characterize the impact of varying the process parameters on the process outcomes such as conversion, partitioning, and mass transfer of all the species between the organic and aqueous layers.

In these experiments, the solvent ratio of MeTHF to 2 N aqueous HCl solution was varied up to ±15% while the total solvent amount was kept constant, the amount of aqueous HCl solution was varied between 10 to 15 L/kg of Boc-D-leucine starting material supplied to productive reaction, the Boc-D-leucine impurity level was varied up to 2 times the specified limit to reach 95 mol % conversion, and the temperature was kept constant at 20 °C. The experimental design, in which selected parameters were varied, is summarized in Table 2. Each experiment was agitated at 20 °C for 24 h, after which agitation was stopped and the phases were allowed to separate for 24 h. Each phase was quantified for imidazole, morpholine, and MeTHF by gas chromatography (GC), morpholine amide and Boc-D-leucine by UPLC, and water by KF titration. The experimental data (Figure 3) demonstrate no strong correlation between the experimental parameters and partition coefficients. The partition coefficients of morpholine amide, water, and MeTHF showed no correlations within the space explored, and the average value of the experimentally derived partition coefficients was used in the model, as illustrated with red lines in Figure 3. The partition coefficient of morpholine amide was estimated on the basis of experiments 1–7 because of UPLC issues in experiments 8 and 9. Residual imidazole and morpholine were not detected in the organic layer, suggesting full conversion to imidazole·HCl and morpholine·HCl and partitioning into the aqueous layer; therefore, a partition coefficient of 10^{-3} (concentration in the organic phase over that in the aqueous phase) was assumed for these species. Boc-D-leucine was not present in the aqueous layer under the process conditions and remained in the organic phase.

Table 2. Design of Experiments for Characterization of Liquid–Liquid Extraction 1 at 20 °C[a]

		solvent composition (vol %)		amount	
expt	volume of 2 N HCl solution	MeTHF	2 N HCl	morpholine amide	Boc-D-leucine
1	10 V	N	N	N	2×
2		N + 15%	R	N	2×
3		R	N + 15%	N	2×
4		N	N	N	N
5		N	N	N	N
6	12 V	N	N	N	2×
7	15 V	N	N	N	2×
8		R	N + 15%	N	2×
9		R	N − 15%	N	2×

[a]Abbreviations: V, liters of 2 N HCl solution per kilogram of morpholine amide; N, nominal; R, residual (from 100 vol % for constant total solvent amount); 2×, 2 times the elevated impurity concentration.

In the experiments to characterize the mass transfer coefficients, an organic stream representing the nominal process conditions was subjected to liquid–liquid extraction with the standard amount of 2 N aqueous HCl solution. Experiments were performed at 20 °C and at two different agitation levels (nominal and 20% reduced) to assess any sensitivities to mixing speed. Samples of both the organic and aqueous layers were assayed at regular time intervals (1 min, 5 min, 10 min, 1 h, 2 h, and 24 h) after addition of the HCl solution to assess the rate of mass transfer on all species. Figure 4 shows the composition of species in both phases. This study confirmed that mass transfer of all species present in the experiment (solvents, solutes, and water) is instantaneous within the duration relevant to the process. Also, no mixing sensitivity was observed for mass transfer at the two investigated agitation levels. These results confirmed that the mass transfer kinetics was not rate-limiting, and the overall coefficient for mass transfer between the organic and aqueous phases was defined as 1 s^{-1} for all of the species in the process model, so that the partitioning was defined by the equilibrium partition coefficients. A 10 min residence time was implemented in CSTR 4 because of the instantaneous reaction and mass transfer kinetics relative to the residence time and the ease of implementation while having a small reactor volume.

Two reactions are considered in CSTR5: (1) the reaction of Boc-D-leucine with Na_2CO_3 to form Boc-D-Leu-ONa salt and $NaHCO_3$ (eq 9) and (2) the reaction of Na_2CO_3 with HCl to form $NaHCO_3$ and NaCl (eq 10):

$$\text{Na}_2\text{CO}_3 + \text{Boc-D-leucine} \rightarrow \text{Boc-D-Leu-ONa} + \text{NaHCO}_3 \quad (9)$$

$$\text{Na}_2\text{CO}_3 + \text{HCl} \rightarrow \text{NaCl} + \text{NaHCO}_3 \quad (10)$$

Each reaction was confirmed to be fast under basic reaction conditions (<1 min) and reach complete conversion and was assumed to have a high rate constant in the reaction kinetics model to describe fast acid–base reaction kinetics and ensure high conversion in the model.

Following the reaction, the biphasic stream undergoes a liquid–liquid phase separation in DEC2. As described in the previous section, two sets of batch experiments were executed

https://dx.doi.org/10.1021/acs.oprd.0c00187
Org. Process Res. Dev. 2020, 24, 1861–1875

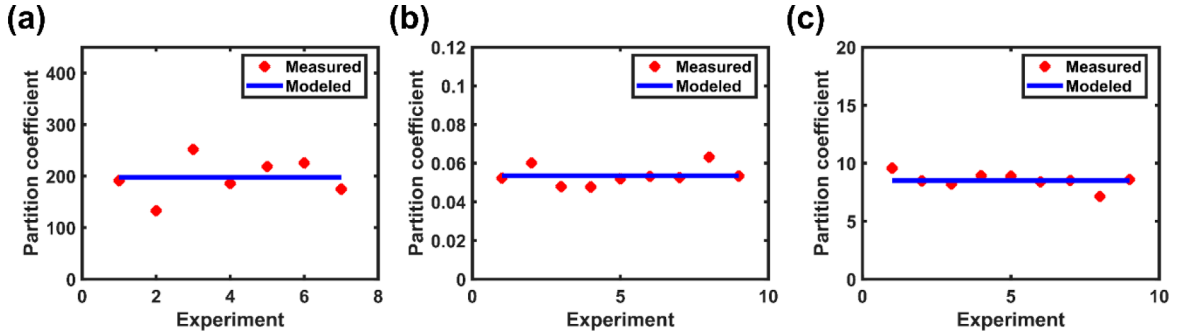

Figure 3. Spread of experimental data for partition coefficients in LLE1 for (a) morpholine amide, (b) water, and (c) MeTHF.

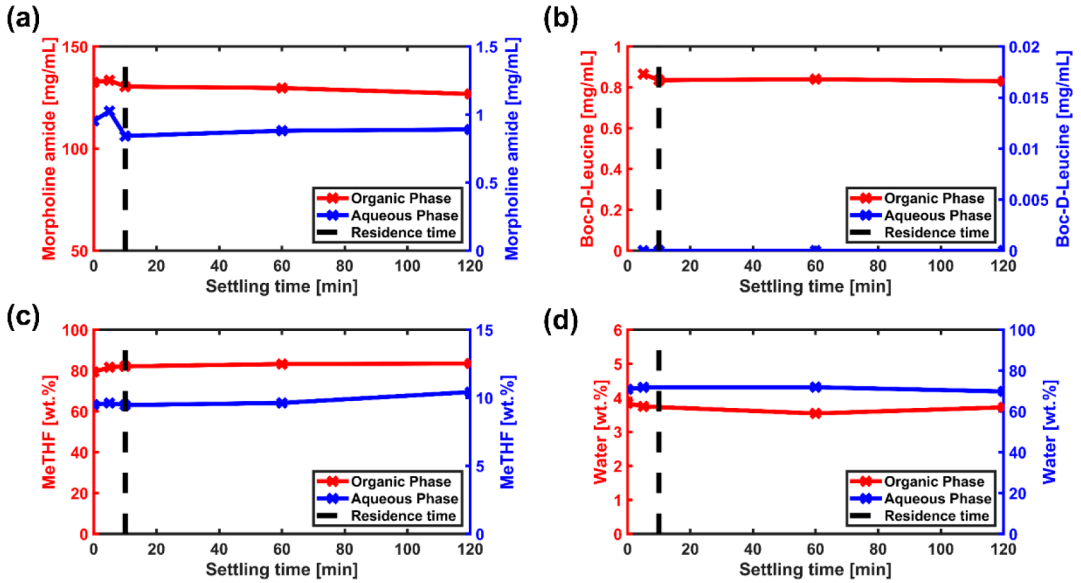

Figure 4. Distributions of (a) morpoholine amide, (b) Boc-D-leucine, (c) MeTHF, and (d) water in the organic and aqueous phases during mass transfer experiments.

to quantify the liquid−liquid phase separation and mass transfer kinetics. These experiments aimed to characterize the impact of the varying process parameters on the process outcomes such as conversion, partitioning, and mass transfer of all the species between the organic and aqueous layers.

In the experiments to characterize the equilibrium partition coefficients, the solvent ratio of MeTHF versus Na_2CO_3 solution was varied up to ±15% of the nominal range while the total solvent amount was kept constant, the Boc-D-leucine impurity level was varied up to 2 times the specified limit to reach 95 mol % conversion, and the temperature was kept constant at 20 °C. The experimental design, in which selected parameters were varied, is summarized in Table 3. Similar to the previous liquid−liquid extraction, each experiment was agitated at 20 °C for 24 h, after which agitation was stopped and the phases were allowed to separate for 24 h. Each phase was quantified for MeTHF by GC, morpholine amide and Boc-D-leucine by UPLC, and water by Karl Fisher titration. In the experimental data, no strong correlation was identified between the experimental parameters (impurity and product concentration, water vs MeTHF composition) and the partition coefficients. The experimental data for partitioning of morpholine amide, water, and MeTHF between the organic and aqueous phases are shown in Figure 5. The partition coefficients of morpholine amide, water, and MeTHF were assumed to be constant, and the average values of the experimentally determined partition coefficients were used in the model, which are shown with the blue lines in Figure 5. No residual Boc-D-leucine was detected in the organic layer, suggesting complete conversion into the salt form and partitioning into the aqueous layer, so a partition coefficient of 10^{-3} (organic phase concentration over aqueous phase concentration) was assumed. All of the other species were assumed to have partition coefficients of 10^{-3} (organic phase concentration over aqueous phase concentration).

Mass transfer experiments were conducted in a manner identical to that described for the previous aqueous workup. Mass transfer was determined to be immediate on time scales relevant to the process (<1 min), and no sensitivity to mixing

Table 3. Design of Experiments for Characterization of Liquid−Liquid Extraction 2 at 20 °C[a]

	solvent composition (vol %)		amount	
expt	MeTHF	8 wt % Na_2CO_3	morpholine amide	Boc-D-leucine
1	N	N	1×	1×
2	N + 15%	R	1×	1×
3	N − 15%	R	1×	1×
4	N	N	1×	2×

[a]Abbreviations: N, nominal; R, residual; 1×, nominal concentration; 2×, 2 times the elevated impurity concentration.

https://dx.doi.org/10.1021/acs.oprd.0c00187
Org. Process Res. Dev. 2020, 24, 1861−1875

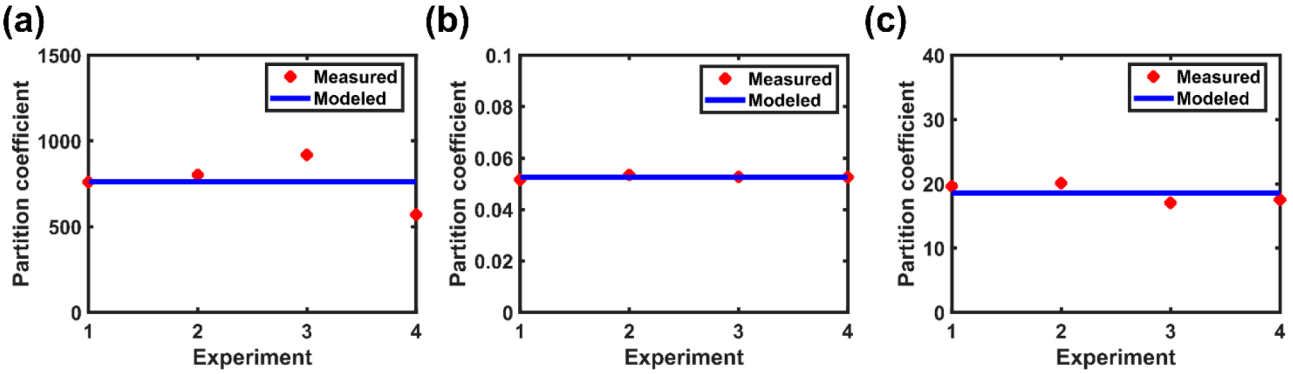

Figure 5. Spread of experimental data for partition coefficients in LLE2 for (a) morpholine amide, (b) water, and (c) MeTHF.

was observed at the two investigated agitation levels. This confirmed that the mass transfer kinetics was not rate-limiting, and the overall mass transfer coefficient between the organic and aqueous phases was defined as 1 s^{-1} for all of the species in the process model, so that the partitioning was defined by the equilibrium partition coefficients. Increasing the residence time in CSTR 5 above its base value was not needed because of the relatively instantaneous reaction and mass transfer kinetics.

3.1.3. Distillation Process Characterization and Model Development. The final unit operation is an azeotropic distillation to remove water from the organic stream containing morpholine amide **3**, MeTHF, and water. The target water content after distillation is ≤0.25 wt % to ensure productivity in the water-sensitive Step 2 Grignard process.[33] In addition to the water content, the potency of this organic stream must meet a composition of 45−55 wt % **3** for compatibility with the downstream operation. To meet these requirements, a distillation process was designed to benefit from the azeotrope behavior of water and MeTHF.[34] The distillation temperature must be kept below 40 °C to avoid morpholine amide decomposition, and the target pressure is below 200 mbar. Batch, semibatch, and truly continuous distillation operations were evaluated computationally. Both batch and continuous operations were demonstrated for model verification; additionally, continuous operation was demonstrated in a production-scale run. All of the models used nonrandom two-liquid (NRTL) binary interaction parameters for MeTHF and water to describe the temperature-dependent vapor−liquid equilibrium data.[34] The distillation models assumed fast mass transfer of MeTHF and water between the liquid and vapor phases, with an overall volumetric mass transfer coefficient specified at 1 s^{-1}, and morpholine amide and any other impurities were treated as nonvolatile species. Heat transfer properties were estimated separately for the various distillation equipment (reactor, rotary evaporator, and distillation column).

The operation of the batch distillation was as follows: A fixed volume of process solution was added to the reactor, and solvent was then evaporated until the volume within the apparatus was below a specified level. A fixed amount of solvent was then added, and the solution was evaporated to a specified volume. The product solution was then discharged for dilution with THF. The batch distillation process, including volumes and amount of solvent added, was developed in silico using the DynoChem solvent swap model. This batch procedure was then verified experimentally to ensure that both the water (0.089 wt %) and concentration (51 wt % **3**) requirements were met.

The semibatch procedure was designed in silico to use an automated rotary evaporator apparatus to repeat the batch distillation cycles and enable integration with upstream and downstream continuous flow steps. The semibatch distillation process was modeled in the virtual plant using the gPROMS distillation drum model integrated with scheduling task functionality to represent automated semibatch process operation. Rotary evaporators are popular equipment choices in chemical research laboratories because of their ease of operation and convenience for small- and medium-scale distillations, but the separation performance of these evaporators is limited because they are based on a single vapor−liquid equilibrium stage. Additionally, the semibatch nature of the process creates limitations in real-time manipulations of distillation conditions to control quality attributes, limiting our ability to develop an end-to-end control strategy.

To achieve a truly continuous process with good separation performance through several vapor−liquid equilibria[35] and to overcome operational challenges associated with semibatch operation, a packed bed distillation column was evaluated in silico and implemented on a production scale. The operation was as follows: The process solution was fed to the column along with a stream of MeTHF. The reflux ratio was used to control the concentration of morpholine amide solution leaving the bottom of the column, and the reboiler duty was used to control the maximum temperature in the column. For the virtual plant, a distillation column model custom-developed by Process Systems Enterprise (PSE) was used. For the packed column, packing material specifications for Pro-Pak 0.24 in. protruded packing from the vendor were used,[36] and experimental data were used to estimate the temperature profile and pressure drop across the column.

3.2. Computational Methods. Reaction kinetic parameters were determined in DynoChem 5[37] software using solution chemistry: a simple batch reaction model. Kinetic parameters for CSTR1 and CSTR2 were estimated using concentration measurements for both the reactant and product. Kinetic parameters for the quench reaction in CSTR3 were confirmed to be fast and were not calibrated. The reactions occurring in CSTR4 and CSTR5 were instantaneous and not calibrated. Partition coefficients for the liquid−liquid equilibria in DEC1 and DEC2 were modeled as the average values from all of the experimental data. Mass transfer coefficients for the liquid−liquid equilibria in DEC1 and DEC2 were confirmed to be sufficiently large and were not estimated. For the distillation drum, the mass transfer

https://dx.doi.org/10.1021/acs.oprd.0c00187
Org. Process Res. Dev. 2020, 24, 1861−1875

coefficients were assumed to be large and were not otherwise characterized.

The end-to-end simulation was created in PSE gPROMS FormulatedProducts, version 1.4.[38] A database containing physical and thermodynamic properties of proprietary and other compounds was developed using gPROMS FormulatedProducts Utilities and MultiFlash 6.1. NRTL activity coefficients describing the vapor−liquid equilibria of water and MeTHF were obtained from Dechema.[34] All of the unit operations, including CSTRs, decanters, the distillation drum, and distillation column units, were modeled by the gPROMS FormulatedProducts standard and custom library models. The operation was made with tasks that mirrored expected operation conditions.

For level control within each relevant unit operation, the outflow condition in each relevant unit operation was controlled with the fixed-volume specification. For temperature control in each relevant unit operation, the embedded model was used to modify the temperature of the incoming heat transfer fluid. Heat transfer coefficients were estimated to be 4.56 W/K for glass reactors using DynoChem Utilities.

For disturbance analysis, the simulation was run with nominal conditions to reach steady state (10 000 s), unless otherwise specified. Following this, disturbances were introduced as step changes and allowed to run to steady state. Process disturbances were determined on the basis of expected fluctuations at scale, and model disturbances were determined on the basis of either (1) the standard deviation of the determined parameters or (2) the largest difference between the model prediction and experimental data in the calibration set.

4. PROCESS DISTURBANCE ANALYSIS

After models were developed for the individual unit operations, they were connected in a flowsheet-level integrated model including regulatory control loops for dynamic simulation. The simulation was then used to perform disturbance analysis and to determine how disturbances would impact downstream unit operations, especially the critical quality attributes (CQAs). This allowed determination of the critical process parameters (CPPs) that impacted the CQAs and guided the development of a process control strategy to ensure that the operating parameters delivered to these quality targets. The target-level process specifications were initially developed for the batch process and were targeted by the continuous process. Uncertainties fell into two distinct groups: (i) process uncertainties and (ii) model uncertainties. Process uncertainties in the form of operational disturbances included disturbances in flow rate and composition of the feed stream as well as the temperature and fill levels in every unit operation. Operational disturbances along with the allowed tolerances are shown in Table 4. Model uncertainties included parametric uncertainties of the estimated kinetic and thermodynamic parameters. Model uncertainties along with the allowed tolerance for each parameter are shown in Table 5. For uncertainty in the reaction kinetics, a tolerance of ±10% was chosen as an approximation of the uncertainty in the 95% confidence interval hyperellipsoid that allows for better interpretability by only changing one parameter at a time. All of the process parameters were recorded in the simulation, but the major focus of this analysis was the conversion of Boc-D-leucine leaving CSTR3, a CQA.

Table 4. Considered Uncertainties in the Form of Operational Disturbances for the Manufacture of Morpholine Amide from Boc-D-leucine

stream/unit operation	variable	allowed tolerance
CDI slurry in MeTHF	flow rate	±10% of total flow rate
CDI slurry in MeTHF	molarity of CDI	±10% of total molarity
Boc-D-leucine monohydrate solution in MeTHF	flow rate	±10% of total flow rate
Boc-D-leucine monohydrate solution in MeTHF	molarity of Boc-D-leucine	±10% of total molarity
morpholine	flow rate	±10% of total flow rate
2 N HCl	flow rate	±10% of total flow rate
2 N HCl	molarity of HCl	±10% of total molarity
8 wt % Na_2CO_3	flow rate	±10% of total flow rate
8 wt % Na_2CO_3	weight fraction of Na_2CO_3	±10% of total molarity
CSTR1	temperature	±5 °C
CSTR1	fill level	±10% of Reactor Volume
CSTR2	temperature	±5 °C
CSTR2	fill level	±10% reactor volume
CSTR3	temperature	±5 °C
CSTR3	fill level	±10% of reactor volume
CSTR4	fill level	±10% of reactor volume
CSTR5	fill level	±10% of reactor volume

Table 5. Considered Model Uncertainties in the Form of Parametric Uncertainties for the Manufacture of Morpholine Amide from Boc-D-leucine

stream/unit operation	variable	allowed tolerance
CSTR1/CSTR2	forward reaction rate	±10% of absolute value
DEC1	imidazole partition coefficient	±10% of absolute value
DEC1	morpholine partition coefficient	±10% of absolute value
DEC1	imidazole-HCl partition coefficient	±10% of absolute value
DEC1	morpholine amide partition coefficient	+28/−33% of absolute value
DEC1	water partition coefficient	+18/−11% of absolute value
DEC1	MeTHF partition coefficient	+12/−17% of absolute value
DEC1	HCl partition coefficient	+18/−11% of absolute value
DEC2	Boc-D-leucine partition coefficient	±10% of absolute value
DEC2	Morpholine amide partition coefficient	+21/−25% of absolute value
DEC2	Water partition coefficient	±1% of absolute value
DEC2	MeTHF partition coefficient	±8% of absolute value
DEC2	Na_2CO_3 partition coefficient	±1% of reactor volume
DEC2	NaCl partition coefficient	±10% of absolute value
DEC2	$NaHCO_3$ partition coefficient	±10% of absolute value
DEC2	HCl partition coefficient	±10% of absolute value

The step response matrices for the conversion of Boc-D-leucine leaving CSTR3 are shown in Figure 6. The plot shows

https://dx.doi.org/10.1021/acs.oprd.0c00187
Org. Process Res. Dev. 2020, 24, 1861−1875

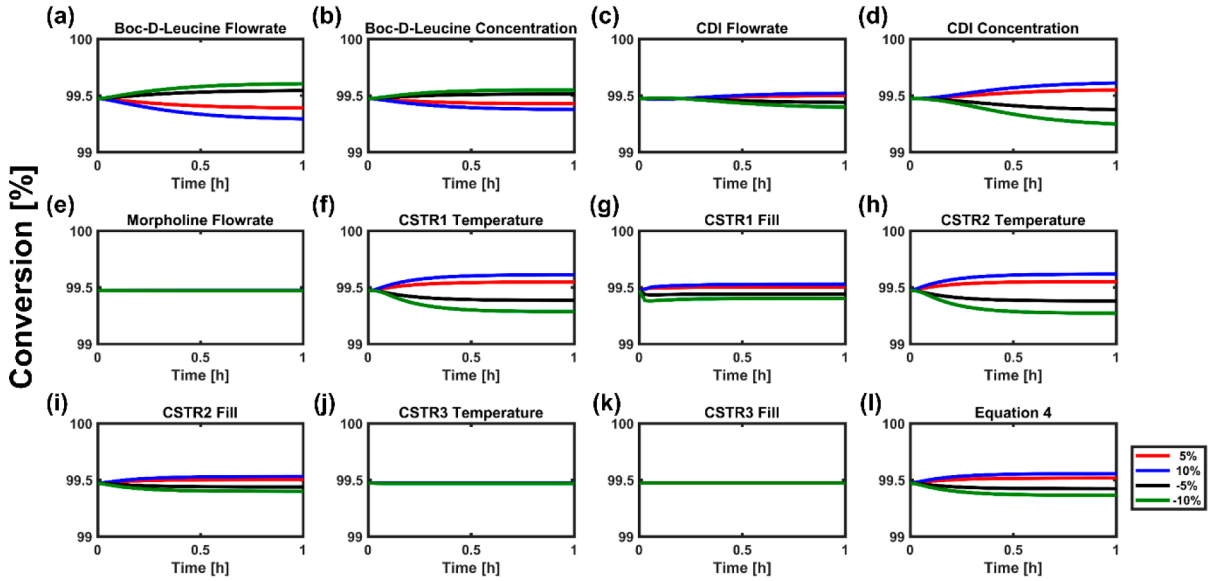

Figure 6. Conversion of Boc-D-leucine in CSTR3 as a function of operational parameters for (a) Boc-D-leucine flow rate, (b) Boc-D-leucine concentration, (c) CDI flow rate, (d) CDI concentration, (e) morpholine flow rate, (f) CSTR1 temperature, (g) CSTR1 fill level, (h) CSTR2 temperature, (i) CSTR2 fill level, (j) CSTR3 temperature, (k) CSTR3 fill level, and (l) eq 4 pre-exponential factor.

the impact of one parameter at a time on the conversion of Boc-D-leucine. For each parameter, a disturbance within the predefined allowed tolerances was applied at four levels: nominal plus the maximum tolerance, nominal plus half the maximum tolerance, nominal minus half the maximum tolerance, and nominal minus the maximum tolerance. As shown, operational disturbances in the Boc-D-leucine flow rate, CDI concentration, CSTR1 temperature, and CSTR2 temperature have a strong impact on conversion, while operational disturbances in the Boc-D-leucine concentration, CDI flow rate, CSTR1 fill level, and CSTR2 fill level and model uncertainty in the CSTR1 rate constant have a moderate impact on conversion. All of the other disturbances and uncertainties have negligible impacts on the conversion of CSTR3.

The total impact and relative ordering of the impacts of these operational disturbances and model uncertainties are illustrated in a tornado diagram (Figure 7). As expected, larger changes in conversion are caused by process uncertainties that couple changes in supplied reactants and total flow rate. As an example, increasing the CDI concentration increases the amount of CDI without changing the CSTR residence time or Boc-D-leucine concentration, but increasing the CDI flow rate increases the amount of CDI at the expense of residence time and total Boc-D-leucine concentration. Additionally, the rapid reaction kinetics for the formation of morpholine amide **3** in CSTR3 enables complete conversion in shorter times than the residence time defined in the unit operation. Therefore, the fill level and temperature in CSTR3 have negligible effects. Also, morpholine is supplied in excess molar quantities, so the conversion is insensitive to the morpholine flow rate.

The process is shown to be very robust, and the conversion is greater than 95% for all cases. To develop a control strategy and to determine whether feedback control is required, the worst-case scenarios of these disturbances were studied, and the results are summarized in Figure 8. The combined impact

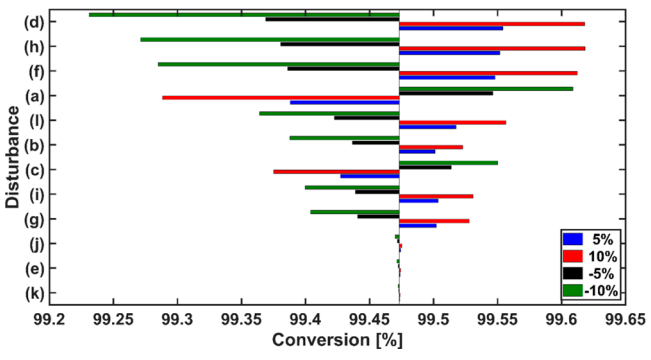

Figure 7. Tornado diagram for the conversion of Boc-D-leucine in CSTR3 with respect to disturbances in (a) Boc-D-leucine flow rate, (b) Boc-D-leucine concentration, (c) CDI flow rate, (d) CDI concentration, (e) morpholine flow rate, (f) CSTR1 temperature, (g) CSTR1 fill level, (h) CSTR2 temperature, (i) CSTR2 fill level, (j) CSTR3 temperature, (k) CSTR3 fill level, and (l) CSTR1/CSTR2 pre-exponential factor.

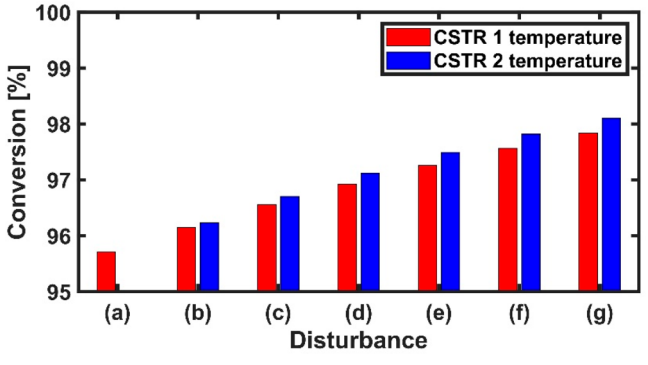

Figure 8. Conversion of Boc-D-leucine for (a) the worst-case scenario of disturbances, (b) increased CSTR1/CSTR2 temperature (17.5 °C actual), (c) increased CSTR1/CSTR2 temperature (20 °C), (d) increased CSTR1/CSTR2 temperature (22.5 °C), (e) increased CSTR1/CSTR2 temperature (25 °C), (f) increased CSTR1/CSTR2 temperature (27.5 °C), and (g) increased CSTR1/CSTR2 temperature (30 °C).

https://dx.doi.org/10.1021/acs.oprd.0c00187
Org. Process Res. Dev. 2020, 24, 1861−1875

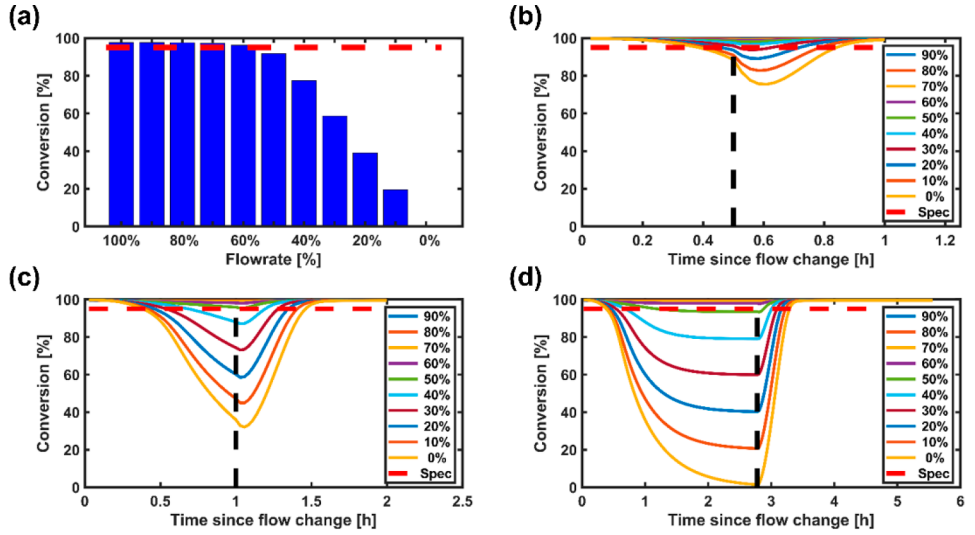

Figure 9. (a) Boc-D-leucine conversion at steady state with reduced CDI flow rates. (b–d) Boc-D-leucine conversion (b) after 30 min of reduced flow rate and 30 min of recovery, (c) after 1 h of reduced flow rate and 1 h of recovery, and (d) after 2.78 h of reduced flow rate and 2.78 h of recovery.

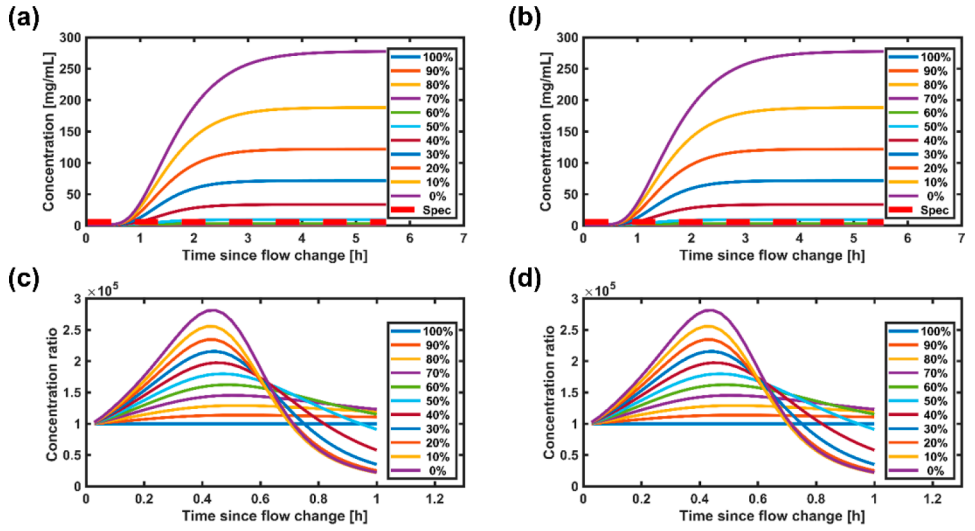

Figure 10. Downstream clearance of Boc-D-leucine. (a) Concentration of Boc-D-leucine leaving LLE1 at various CDI flow rates, with the maximum experimental condition tested shown by the dashed red line. (b) Concentration of Boc-D-leucine leaving LLE1 at various CDI flow rates in less than 1 h, with the maximum experimental condition tested shown by the dashed red line. (c) Mass ratio of morpholine amide to Boc-D-leucine leaving LLE2 at various CDI flow rates. (d) Mass ratio of morpholine amide to Boc-D-leucine leaving LLE2 at various CDI flow rates in less than 1 h.

of the worst-case scenarios is shown in Figure 8a, which demonstrates all of the disturbances shown in Figure 7 happening at the same time in their worst cases, and the conversion remains greater than 95%. While the probability of a combination of several worst-case scenarios happening at the same time is low, the temperatures of CSTR1 and CSTR2 serve as levers to increase the reaction conversion in the case of an operational disturbance because (1) they are easily controllable and (2) they can increase the conversion in the worst-case scenario by 2% through an increase of 10 °C.

4.1. Case Study: CDI Slurry Blockage. While the process is robust toward disturbances and uncertainties under normal operation, a partial or total blockage of the CDI feed slurry was identified as a possible failure scenario. Such blockages could be dynamic or accumulate gradually, and therefore, both the dynamic and steady-state operation for different failure modes required analysis. Figure 9 illustrates the steady-state and dynamic conversion of Boc-D-leucine leaving CSTR2 under different blockage scenarios. The desired level of conversion (>95%) is attained at flow rates as low as 60% of the nominal set point. Below this point, the conversion is impacted at varying rates and magnitudes. For example, >95% conversion of Boc-D-leucine can be maintained if a 70% blockage (i.e., the CDI flow rate is 30% of the nominal set point) is resolved within 30 min. Alternatively, a blockage persisting for 1 h can accommodate only 50% of the nominal flow. An unexpected observation made possible by the dynamic model is that resuming the CDI flow results in a temporary reduction in conversion due to a reduction in residence time. Furthermore, the integrated nature of this analysis demonstrated that the system can tolerate deviations in which excess Boc-D-leucine is present (Figure 10). That is, the incorporation of a basic quench in CSTR5 converts most of the Boc-D-leucine to the

https://dx.doi.org/10.1021/acs.oprd.0c00187
Org. Process Res. Dev. 2020, 24, 1861–1875

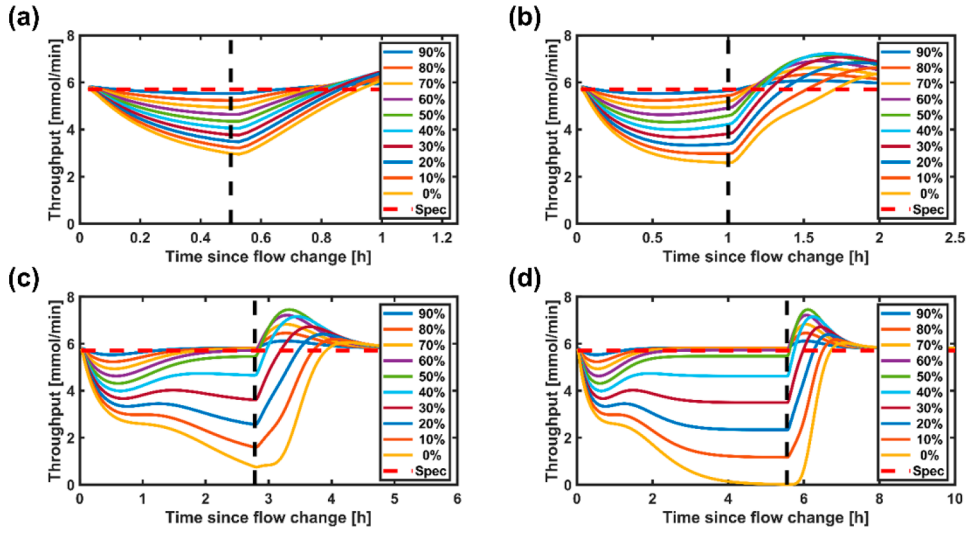

Figure 11. Amount of morpholine amide entering the hold tank prior to distillation at various CDI flow rates along with flow recovery at (a) 0.5 h, (b) 1 h, (c) 2.78 h, and (d) 5.56 h.

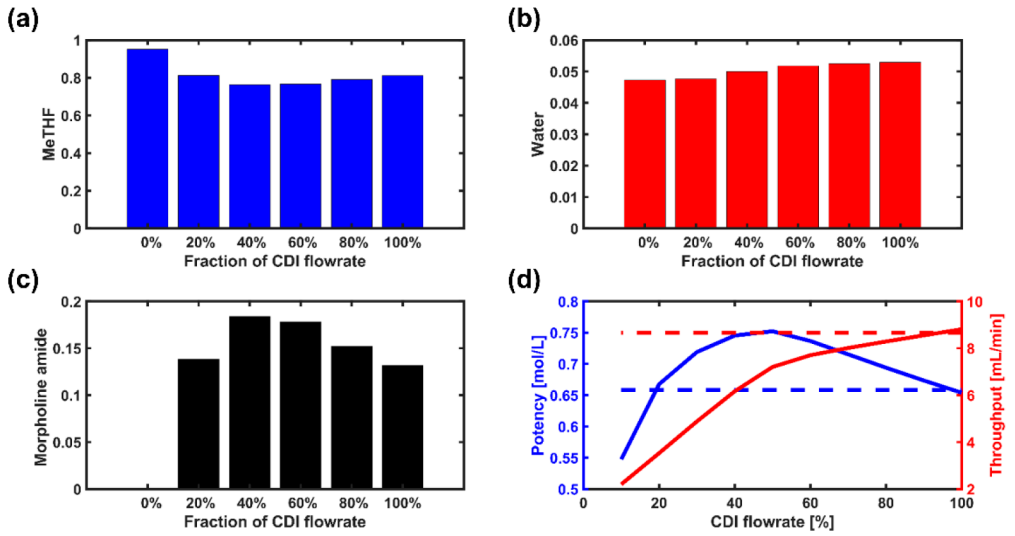

Figure 12. (a–c) Mass fractions of (a) MeTHF, (b) water, and (c) morpholine amide entering the hold tank prior to distillation at various CDI flow rates. (d) Formulated morpholine amide potency (blue) and throughput (red) after semibatch distillation at various CDI flow rates.

water-soluble Boc-D-Leu-ONa salt, which preserves the relative purity of the morpholine amide product **3**.

Finally, even though the upstream process supplies a high-purity organic stream, CDI flow rate changes and therefore deviations in the morpholine amide potency and flow rate could impact the distillation unit operation. The impact of the morpholine amide stream flow rate (mmol/min) on the distillation operation is shown in Figure 11. The interesting dynamics is shown to describe the impact of CDI flow rate reductions of various durations on the morpholine amide stream flow rate (mmol/min) entering the hold tank prior to the distillation operation. As shown in Figure 11a,b, blockage of the CDI feed stream decreases the total amount of morpholine amide entering the hold tank. This response is due to a lower total flow rate supplied through the system, which increases the residence time and results in less throughput. If the blockage is long enough (>1 h), the flow rate approaches the new steady-state conversion of Boc-D-leucine, as shown in Figure 11c,d. In each case, upon recovery of the CDI flow rate, there is a spike in the amount of morpholine amide entering the hold tank due to an increased total flow rate through the system.

Understanding how this hold tank dynamics is correlated to the final morpholine amide feed to Step 2 is critical to developing a control strategy. Figure 12 examines the hold tank composition prior to the distillation operation and the molar concentration and production rate (mL/min) of morpholine amide after the semibatch distillation operation at steady state for various changes in CDI flow rate. The steady-state mass fractions of morpholine amide, MeTHF, and water in the hold tank stream prior to distillation at different CDI blockage scenarios are shown in Figure 12a–c. For example, when the CDI flow rate decreases to 60% of its nominal value, the morpholine amide concentration in the hold tank increases, whereas the MeTHF and water contents decrease. There are two reasons for a difference in the composition change trends of the product and the solvents. Morpholine amide synthesis is still achieved at >95% conversion of Boc-D-leucine up to a CDI flow rate drop of 40%, resulting in a constant amount of morpholine amide generated. However, a decrease in CDI flow

https://dx.doi.org/10.1021/acs.oprd.0c00187
Org. Process Res. Dev. 2020, 24, 1861–1875

rate results in a decreased overall flow rate of MeTHF in the process and a lower hold-tank fill rate, which increases the concentration of the morpholine amide product in solution while reducing the solvent content. Thus, a CDI flow rate reduction to 60% increases the total morpholine amide concentration in the hold tank and decreases the overall throughput. Below 60% of the nominal flow rate of CDI, the morpholine amide concentration in the hold tank and the formulated product and the total morpholine amide flow rate decrease as the Boc-D-leucine conversion decreases.

In the case of a semibatch distillation operation, this decreased throughput and varying (first increased than decreased) concentration of morpholine amide propagate downstream to the Step 2 feed stream. This response is due to the nature of the semibatch distillation operation and having fixed-volume charges processed in each batch. The impact of CDI flow rate changes on the formulated morpholine amide potency and throughout after semibatch distillation are shown in Figure 12d. The amount of MeTHF supplied to the system forces the total throughput to decrease below the desired value, which correlates to a reduced feed stream flow rate and a higher-concentration stream being supplied to the Step 2 process for CDI blockages up to 60%. This deviation in formulated morpholine amide concentration can be addressed by adding a UPLC that measures the morpholine amide concentration in the hold tank. The measurement from this UPLC can then be used to control the MeTHF flow rate to the hold tank to dilute the morpholine amide to its desired potency. Alternatively, dilution of the morpholine amide stream can also be done simultaneously with the THF formulation postdistillation to reduce the number of UPLCs required for the process.

An alternative approach is to replace the semibatch distillation drum operation with a truly continuous distillation column operation that can tolerate variations in product concentration and still process the solution to meet the desired specifications. This approach was explored with a different version of the virtual plant model by incorporating a packed bed distillation column model as described previously. The disturbances of potency and composition changes in the morpholine amide feed for the distillation column can be overcome by manipulating the reflux ratio and feed flow rate into the column and by controlling the water content and morpholine amide concentration at the outlet of the distillation column (as confirmed with in silico results). Compared with the batch distillation drum, the continuous distillation column was found to be more robust toward process upsets such as deviations in the morpholine amide concentration leaving DEC2. This increased robustness was largely a result of the greater amount of instrumentation required for control of continuous distillation processes. This instrumentation provided more feedback for the process, which allowed for faster recognition of and responses to process upsets. These results supported the implementation of continuous distillation at the production scale.

4.2. Production-Scale Demonstration. The integrated continuous process to produce morpholine amide **3** was demonstrated for 48 h using production-scale equipment. The disturbance analysis results were used to make process decisions for how long to sustain blockages of the CDI flow and when to divert the process stream to waste. The flow rates of all feed streams were monitored by mass flow meters, and a disruption in the CDI flow rate was observed at the 16 h time point. As described in the previous section, the disturbance analysis for CDI blockage supported a continuation of operation, provided that the blockage was resolved within 30 min. In actual production, the blockage was detected and resolved within 22 min of occurrence, and therefore, all of the other flow rates were maintained at the nominal set points, and material was continuously fed through the entire system. The concentrations of residual starting material Boc-D-leucine in CSTR3 and CSTR5 are shown in Figure 13. The target of 95%

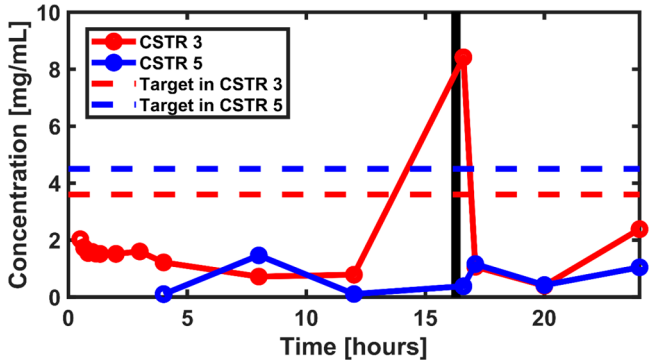

Figure 13. Production-scale demonstration data for the Boc-D-leucine concentrations in CSTR3 and CSTR5. The concentrations corresponding to the 95% conversion target are shown as dashed lines for CSTR3 and CSTR5. The black bar indicates the CDI flow disturbance duration of 22 min.

conversion corresponds to Boc-D-leucine concentrations of 3.6 and 4.6 mg/mL in CSTR3 and CSTR5, respectively. An increased Boc-D-leucine concentration in CSTR5 is observed because of partitioning of MeTHF into the aqueous phase in the liquid–liquid extractions that result in concentration of organic layer. An increase in Boc-Leu-OH content to 8.4 mg/mL is observed in CSTR3 upon CDI blockage and is purged in the basic aqueous quench (CSTR5), as shown in Figure 13. Both the duration and magnitude of Boc-D-leucine excursion are in agreement with the disturbance analysis for CDI blockage scenarios. These predictions are shown in Figure 14 and are in excellent alignment with the pilot-plant operation.

A distillation column unit operation was utilized to achieve truly continuous operation and to buffer the concentration

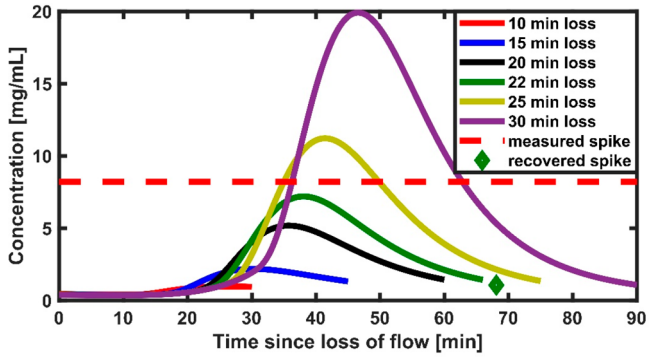

Figure 14. Boc-D-leucine concentration in CSTR3 at various durations of CDI flow blockage. The red dashed line represents the maximum measured concentration during a 22 min flow blockage in the production run. The green dot represents the measurement in CSTR3 following flow recovery. The measurement was taken 30 min after the spike, and the dot is plotted to reflect this.

https://dx.doi.org/10.1021/acs.oprd.0c00187
Org. Process Res. Dev. 2020, 24, 1861–1875

variations inherent to the upstream process, including disturbances in CDI flow. Integration of the distillation column enabled us to successfully achieve the target end points for both water content (<2500 ppm) and morpholine amide concentration (45−55 wt %) for all materials collected (Figure 15).

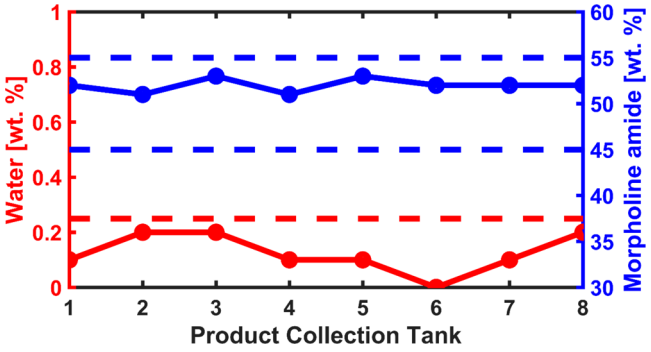

Figure 15. Morpholine amide potency and water content in the final product collection tank in the integrated Step 1 production-scale demonstration. The blue dashed lines indicate the upper and lower limits for morpholine amide potency, and the red dashed line indicates the upper limit for water content.

5. CONCLUSIONS AND FUTURE WORK

This article has described the development of a virtual plant to characterize and build a robust process control strategy for the preparation of morpholine amide **3** by an integrated continuous process consisting of eight unit operations. The individual unit operation models were built separately and then integrated into an end-to-end dynamic flowsheet model that was used to determine the impact of process and model uncertainties on product quality specifications. It was found that the process is robust toward expected disturbances and uncertainties but that blockages of the CDI slurry stream can impact the Boc-D-leucine conversion and final morpholine amide potency. Integration of the distillation column unit operation was a key step in the updated process control strategy to achieve target end-point product specifications. These predictions were verified through production-scale demonstrations and highlight the benefits of mathematical modeling as a predictive tool to understand pharmaceutical continuous manufacturing processes. This type of in silico process characterization represents a powerful approach for achieving optimal operating conditions while reducing the amount of experimentation required to expand process knowledge.

The virtual plant model created in this work facilitates science- and risk-based implementation of continuous manufacturing. This includes the development of advanced process control strategies and identification of optimal operation policy such as approaches to throughput and product collection/diversion that are in line with the ICH Q13 guidance goals.[39] The development of a virtual plant for synthetic CM has enabled us to successfully predict process performance and product quality in a real plant environment. The prediction accuracy of our model helps to deliver more reliable processes, use human and capital resources more efficiently, and establish an agile process development paradigm as a differentiating capability in our industry.

AUTHOR INFORMATION

Corresponding Author

Elçin Içten − *Process Development, Amgen, Inc., Cambridge, Massachusetts 02142, United States;* orcid.org/0000-0002-0962-7550; Email: eicten@amgen.com

Authors

Andrew J. Maloney − *Department of Chemical Engineering, Massachusetts Institute of Technology, Cambridge, Massachusetts 02139, United States;* orcid.org/0000-0002-9744-6433

Matthew G. Beaver − *Process Development, Amgen, Inc., Cambridge, Massachusetts 02142, United States;* orcid.org/0000-0003-3816-4601

Dongying Erin Shen − *Process Development, Amgen, Inc., Cambridge, Massachusetts 02142, United States*

Xiaoxiang Zhu − *Process Development, Amgen, Inc., Cambridge, Massachusetts 02142, United States*

Lauren R. Graham − *Process Development, Amgen, Inc., Cambridge, Massachusetts 02142, United States*

Jo Anna Robinson − *Process Development, Amgen, Inc., Cambridge, Massachusetts 02142, United States*

Seth Huggins − *Process Development, Amgen, Inc., Thousand Oaks, California 91320, United States*

Ayman Allian − *Process Development, Amgen, Inc., Thousand Oaks, California 91320, United States*

Roger Hart − *Process Development, Amgen, Inc., Cambridge, Massachusetts 02142, United States*

Shawn D. Walker − *Process Development, Amgen, Inc., Cambridge, Massachusetts 02142, United States;* orcid.org/0000-0001-8827-4679

Pablo Rolandi − *Process Development, Amgen, Inc., Cambridge, Massachusetts 02142, United States*

Richard D. Braatz − *Department of Chemical Engineering, Massachusetts Institute of Technology, Cambridge, Massachusetts 02139, United States;* orcid.org/0000-0003-4304-3484

Complete contact information is available at: https://pubs.acs.org/10.1021/acs.oprd.0c00187

Notes

The authors declare no competing financial interest.

ACKNOWLEDGMENTS

The authors acknowledge Meera Mahadevan, Ananya Chowdhury, and Kevin Healy from Process Systems Enterprise Ltd. for their support on gPROMS models; Ryan Woods, Chris Dicus, Alec Gordon, Taquasia Hepburn, and Olivier Dapremont from Ampac Fine Chemicals for production-scale demonstration of the integrated process; and Gerard Capellades Mendez from MIT for the scientific discussions. The contribution of A.J.M. was partially supported by the National Science Foundation Graduate Research Fellowship under Grant 1122374. Any opinion, findings, and conclusions or recommendations expressed in this material are those of the authors(s) and do not necessarily reflect the views of the National Science Foundation.

ABBREVIATIONS

ACN, acetonitrile; AcOH, acetic acid; CDI, *N*,*N*-carbonyldiimidazole; CM, continuous manufacturing; CO_2, carbon dioxide; CPP, critical process parameter; CQA, critical quality

https://dx.doi.org/10.1021/acs.oprd.0c00187
Org. Process Res. Dev. 2020, 24, 1861−1875

attribute; CSTR, continuously stirred tank reactor; cGMP, current good manufacturing practice; DEC, decanter; FTIR, Fourier transform infrared spectroscopy; GC, gas chromatography; HCl, hydrochloric acid; HPLC, high-performance liquid chromatography; IPC, in-process control; LLE, liquid−liquid extraction; MeOH, methanol; MeTHF, 2-methyltetrahydrofuran; Mn, manganese; MTBE, methyl *tert*-butyl ether; PAT, process analytical technology; QbC, quality by control; QbD, quality by design; SSQ, sum of squares; TBD, triazabicyclodecene; UPLC, ultraperformance liquid chromatography

REFERENCES

(1) Konstantinov, K. B.; Cooney, C. L. White Paper on Continuous Bioprocessing May 20−21, 2014 Continuous Manufacturing Symposium. *J. Pharm. Sci.* **2015**, *104* (3), 813−820.

(2) *Quality Considerations for Continuous Manufacturing—Guidance for Industry*. U.S. Food and Drug Administration, February 2019. https://www.fda.gov/media/121314/download (accessed 2020-04-15).

(3) Byrn, S.; Futran, M.; Thomas, H.; Jayjock, E.; Maron, N.; Meyer, R. F.; Myerson, A. S.; Thien, M. P.; Trout, B. L. Achieving Continuous Manufacturing for Final Dosage Formation: Challenges and How to Meet Them May 20−21, 2014 Continuous Manufacturing Symposium. *J. Pharm. Sci.* **2015**, *104* (3), 792−802.

(4) Hong, M. S.; Severson, K. A.; Jiang, M.; Lu, A. E.; Love, J. C.; Braatz, R. D. Challenges and Opportunities in Biopharmaceutical Manufacturing Control. *Comput. Chem. Eng.* **2018**, *110*, 106−114.

(5) Lee, S. L.; O'Connor, T. F.; Yang, X.; Cruz, C. N.; Chatterjee, S.; Madurawe, R. D.; Moore, C. M. V.; Yu, L. X.; Woodcock, J. Modernizing Pharmaceutical Manufacturing: From Batch to Continuous Production. *J. Pharm. Innovation* **2015**, *10*, 191−199.

(6) Su, Q.; Ganesh, S.; Moreno, M.; Bommireddy, Y.; Gonzalez, M.; Reklaitis, G. V.; Nagy, Z. K. A Perspective on Quality-by-Control (QbC) in Pharmaceutical Continuous Manufacturing. *Comput. Chem. Eng.* **2019**, *125*, 216−231.

(7) Baxendale, I. R.; Braatz, R. D.; Hodnett, B. K.; Jensen, K. F.; Johnson, M. D.; Sharratt, P.; Sherlock, J. P.; Florence, A. J. Achieving Continuous Manufacturing: Technologies and Approaches for Synthesis, Workup, and Isolation of Drug Substance May 20−21, 2014 Continuous Manufacturing Symposium. *J. Pharm. Sci.* **2015**, *104* (3), 781−791.

(8) Içten, E.; Giridhar, A.; Taylor, L. S.; Nagy, Z. K.; Reklaitis, G. V. Dropwise Additive Manufacturing of Pharmaceutical Products for Melt-Based Dosage Forms. *J. Pharm. Sci.* **2015**, *104* (5), 1641−1649.

(9) Srai, J. S.; Badman, C.; Krumme, M.; Futran, M.; Johnston, C. Future Supply Chains Enabled by Continuous Processing-Opportunities and Challenges May 20−21, 2014 Continuous Manufacturing Symposium. *J. Pharm. Sci.* **2015**, *104* (3), 840−849.

(10) Gutmann, B.; Cantillo, D.; Kappe, C. O. Continuous-Flow Technology - A Tool for the Safe Manufacturing of Active Pharmaceutical Ingredients. *Angew. Chem., Int. Ed.* **2015**, *54* (23), 6688−6728.

(11) Içten, E.; Nagy, Z. K.; Reklaitis, G. V. Process Control of a Dropwise Additive Manufacturing System for Pharmaceuticals Using Polynomial Chaos Expansion Based Surrogate Model. *Comput. Chem. Eng.* **2015**, *83*, 221−231.

(12) Mascia, S.; Heider, P. L.; Zhang, H.; Lakerveld, R.; Benyahia, B.; Barton, P. I.; Braatz, R. D.; Cooney, C. L.; Evans, J. M. B.; Jamison, T. F.; et al. End-to-End Continuous Manufacturing of Pharmaceuticals: Integrated Synthesis, Purification, and Final Dosage Formation. *Angew. Chem., Int. Ed.* **2013**, *52* (47), 12359−12363.

(13) Zhang, P.; Weeranoppanant, N.; Thomas, D. A.; Tahara, K.; Stelzer, T.; Russell, G.; O'Mahony, M.; Myerson, A. S.; Lin, H.; Kelly, L. P.; et al. Advanced Continuous Flow Platform for On-Demand Pharmaceutical Manufacturing. *Chem. - Eur. J.* **2018**, *24* (11), 2776−2784.

(14) Thaisrivongs, D. A.; Naber, J. R.; Rogus, N. J.; Spencer, G. Development of an Organometallic Flow Chemistry Reaction at Pilot-Plant Scale for the Manufacture of Verubecestat. *Org. Process Res. Dev.* **2018**, *22* (3), 403−408.

(15) Marsini, M. A.; Buono, F. G.; Lorenz, J. C.; Yang, B. S.; Reeves, J. T.; Sidhu, K.; Sarvestani, M.; Tan, Z.; Zhang, Y.; Li, N.; et al. Development of a Concise, Scalable Synthesis of a CCR1 Antagonist Utilizing a Continuous Flow Curtius Rearrangement. *Green Chem.* **2017**, *19* (6), 1454−1461.

(16) Goundry, W. R. F.; Dai, K.; Gonzalez, M.; Legg, D.; O'Kearney-McMullan, A.; Morrison, J.; Stark, A.; Siedlecki, P.; Tomlin, P.; Yang, J. Development and Scale-up of a Route to ATR Inhibitor AZD6738. *Org. Process Res. Dev.* **2019**, *23* (7), 1333−1342.

(17) Van Alsten, J. G.; Reeder, L. M.; Stanchina, C. L.; Knoechel, D. J. Continuous Reaction/Crystallization Process for Production of a Hazardous Intermediate. *Org. Process Res. Dev.* **2008**, *12* (5), 989−994.

(18) Acevedo, D.; Jarmer, D. J.; Burcham, C. L.; Polster, C. S.; Nagy, Z. K. A Continuous Multi-Stage Mixed-Suspension Mixed-Product-Removal Crystallization System with Fines Dissolution. *Chem. Eng. Res. Des.* **2018**, *135*, 112−120.

(19) Cole, K. P.; Groh, J. M.; Johnson, M. D.; Burcham, C. L.; Campbell, B. M.; Diseroad, W. D.; Heller, M. R.; Howell, J. R.; Kallman, N. J.; Koenig, T. M.; et al. Kilogram-Scale Prexasertib Monolactate Monohydrate Synthesis under Continuous-Flow CGMP Conditions. *Science* **2017**, *356* (6343), 1144−1150.

(20) Cole, K. P.; Reizman, B. J.; Hess, M.; Groh, J. M.; Laurila, M. E.; Cope, R. F.; Campbell, B. M.; Forst, M. B.; Burt, J. L.; Maloney, T. D.; et al. Small-Volume Continuous Manufacturing of Merestinib. Part 1. Process Development and Demonstration. *Org. Process Res. Dev.* **2019**, *23* (5), 858−869.

(21) Reizman, B. J.; Cole, K. P.; Hess, M.; Burt, J. L.; Maloney, T. D.; Johnson, M. D.; Laurila, M. E.; Cope, R. F.; Luciani, C. V.; Buser, J. Y.; et al. Small-Volume Continuous Manufacturing of Merestinib. Part 2. Technology Transfer and CGMP Manufacturing. *Org. Process Res. Dev.* **2019**, *23* (5), 870−881.

(22) Hu, C.; Testa, C. J.; Wu, W.; Shvedova, K.; Shen, D. E.; Sayin, R.; Halkude, B. S.; Casati, F.; Hermant, P.; Ramnath, A.; et al. An Automated Modular Assembly Line for Drugs in a Miniaturized Plant. *Chem. Commun.* **2020**, *56* (7), 1026−1029.

(23) Wang, Z.; Escotet-Espinoza, M. S.; Ierapetritou, M. Process Analysis and Optimization of Continuous Pharmaceutical Manufacturing Using Flowsheet Models. *Comput. Chem. Eng.* **2017**, *107*, 77−91.

(24) Gao, Z.; Rohani, S.; Gong, J.; Wang, J. Recent Developments in the Crystallization Process: Toward the Pharmaceutical Industry. *Engineering* **2017**, *3* (3), 343−353.

(25) Hirshfield, L.; Içten, E.; Giridhar, A.; Nagy, Z. K.; Reklaitis, G. V. Real-Time Process Management Strategy for Dropwise Additive Manufacturing of Pharmaceutical Products. *J. Pharm. Innovation* **2015**, *10* (2), 140−155.

(26) Lakerveld, R.; Benyahia, B.; Braatz, R. D.; Barton, P. I. Model-Based Design of a Plant-Wide Control Strategy for a Continuous Pharmaceutical Plant. *AIChE J.* **2013**, *59* (10), 3671−3685.

(27) Su, Q.; Moreno, M.; Giridhar, A.; Reklaitis, G. V.; Nagy, Z. K. A Systematic Framework for Process Control Design and Risk Analysis in Continuous Pharmaceutical Solid-Dosage Manufacturing. *J. Pharm. Innovation* **2017**, *12* (4), 327−346.

(28) Içten, E.; Reklaitis, G. V.; Nagy, Z. K. Advanced Control for the Continuous Dropwise Additive Manufacturing of Pharmaceutical Products. *Comput. Aided Chem. Eng.* **2018**, *41*, 379−401.

(29) Icten, E.; Maloney, A. J.; Beaver, M. G.; Zhu, X.; Shen, D. E.; Robinson, J. A.; Parsons, A. T.; Allian, A. D.; Huggins, S.; Hart, R.; et al. A Virtual Plant for Integrated Continuous Manufacturing of a Carfilzomib Drug Substance Intermediate, Part 2: Enone Synthesis via a Barbier-Type Grignard Process. *Org. Process Res. Dev.* **2020**, DOI: 10.1021/acs.oprd.0c00188.

(30) Maloney, A. J.; Icten, E.; Capellades, G.; Beaver, M. G.; Zhu, X.; Graham, L.; Brown, D. B.; Griffin, D. J.; Sangodkar, R.; Allian, A.; et al. A Virtual Plant for Integrated Continuous Manufacturing of a Carfilzomib Drug Substance Intermediate, Part 3: Manganese-

Catalyzed Asymmetric Epoxidation, Crystallization, and Filtration. *Org. Process Res. Dev.* **2020**, DOI: 10.1021/acs.oprd.0c00189.
(31) Siegel, D. S.; Martin, T.; Wang, M.; Vij, R.; Jakubowiak, A. J.; Lonial, S.; Trudel, S.; Kukreti, V.; Bahlis, N.; Alsina, M.; et al. A Phase 2 Study of Single-Agent Carfilzomib (PX-171−003-A1) in Patients with Relapsed and Refractory Multiple Myeloma. *Blood* **2012**, *120* (14), 2817−2825.
(32) Dornan, P.; Anthoine, T.; Beaver, M.; Cheng, G. C.; Cohen, D.; Cui, S.; Lake, W.; Langille, N.; Lucas, S.; Patel, J.; et al. Continuous Process Improvement in the Manufacture of Carfilzomib, Part 1: Process Understanding and Improvements in the Commercial Route to Prepare the Epoxyketone Warhead. *Org. Process Res. Dev.* **2020**, *24* (4), 481−489.
(33) Beaver, M.; Shi, X.; Riedel, J.; Patel, P.; Zeng, A.; Corbett, M.; Robinson, J. A.; Parsons, A.; Cui, S.; Baucom, K.; et al. Continuous Process Improvement in the Manufacture of Carfilzomib, Part 2: An Improved Process for Synthesis of the Epoxyketone Warhead. *Org. Process Res. Dev.* **2020**, *24* (4), 490−499.
(34) *Dechema Chemistry Data Series, Vol. 1*; Deutsche Gesellschaft fur Chemisches Aparatewesen, 2004.
(35) Wankat, P. C. Introduction to Column Distillation. In *Separation Process Engineering*, 3rd ed.; Prentice-Hall, 2007; pp 65−85.
(36) *Pro-Pak Protruded Metal Distillation Packing Brochure*. Cannon Instrument Company, 2016. https://www.cannoninstrument.com/Image/GetDocument/425?language=en (accessed 2020-04-15).
(37) *DynoChem Resources*. https://dcresources.scale-up.com (accessed 2020-04-15).
(38) Process Systems Enterprise. *gPROMS FormulatedProducts*. https://www.psenterprise.com/products/gproms/formulatedproducts (accessed 2020-04-15).
(39) *Final Concept Paper for ICH Q13: Continuous Manufacturing of Drug Substances and Drug Products*. International Council for Harmonisation, November 14, 2018. https://database.ich.org/sites/default/files/Q13_EWG_Concept_Paper.pdf (accessed 2020-04-15).

https://dx.doi.org/10.1021/acs.oprd.0c00187
Org. Process Res. Dev. 2020, 24, 1861−1875